Compartment Fire Near-field Entrainment Measurements

N. A. Dembsey, P. J. Pagni & R. B. Williamson

College of Engineering, University of California at Berkeley, Berkeley, CA 94720, USA

ABSTRACT

A widely accepted consensus on entrainment models for large fires in compartments does not yet exist. To obtain further information on such entrainment rates, 20 full-scale, near-field experiments were conducted. Near-field entrainment occurs when hot layer interface heights are beneath the burner mean flame height so that cold layer entrainment occurs only near the burner surface. A durable compartment, similar to the standard fire test compartment, was designed and used in conjunction with a 0·61 m × 1·22 m porous surface propane burner to produce compartment fires with heat release rates from 330 to 980 kW. Entrainment rates of 0·74–0·98 kg/s were calculated from temperature measurements made within the compartment and in the doorway. The entrainment rates determined here were correlated with values from the literature. This correlation led to two curve fits which modify Zukoski's far-field offset model and can be used to estimate near-field entrainment rates. An offset for the near-field model of Thomas was also developed. The fire plume model of Baum and McCaffrey was found to compare favorably with the entrainment rates determined here.

NOTATION

A_b	Burner area (m^2)
A_v	Vent area $= w_v h_v$ (m^2)
c_p	Specific heat (kJ/kg K)

C	Vent flow coefficient $= 0\cdot68$
D	Hydraulic diameter (m)
D^*	Fire characteristic size $= [Q/(\rho_\infty c_p T_\infty \sqrt{g})]^{2/5} = (Q/1110)^{2/5}$ (m)
g	Gravity $= 9\cdot81$ m/s^2
Gr	Grashof number
h_v	Vent height (m)
H	Compartment height (m)
ΔH_c	Heat of combustion (propane) $= 46\cdot4$ MJ/kg
m	Model/correlation entrainment mass flow rate (kg/s)
m_{av}	Average vent mass flow rate $= 0\cdot5(m_o + m_i)$ (kg/s)
m_e	Experimentally determined entrainment mass flow rate (kg/s)
m_f	Virtual origin entrainment mass flow rate for far-field model (kg/s)
m_i	Vent mass inflow rate (kg/s)
m_m	Vent mixing mass flow rate, net into lower layer (kg/s)
m_o	Vent mass outflow rate (kg/s)
m_p	Propane or fuel mass flow rate (kg/s)
m_r	Variable portion of near-field model $= PZ_e^{3/2}(g\rho_\infty\rho_{fl})^{1/2}$, see eqn (15)
m_{ro}	Variable portion of near-field model with offset $= P(Z_e + Z_n)^{3/2}(g\rho_\infty\rho_{fl})^{1/2}$, see eqn (16)
m_f	Flame tip entrainment mass flow rate (kg/s)
m_w	Boundary layer wall mass flow rate per unit width (kg/m s)
m_{wu}	Upward wall mass flow rate (kg/s)
M	Boundary layer momentum per unit width (kg/s^2)
n	Power for flame height correlation
P	Burner/pool perimeter (m)
Q	Fire heat release rate (kW)
Q_c	Fire convective heat release rate (kW)
Q_{O2}	Fire heat release rate based on oxygen consumption calorimetry (kW)
Q_p	Fire potential heat release rate based on propane mass flow rate $= \Delta H_c m_p$ (kW)
Q_{vc}	Ventilation-controlled heat release rate $= 1\cdot6 A_v h_v^{1/2}$ (kW)
Q_D^*	Fire size $= Q/(\rho_\infty c_p T_\infty \sqrt{g} D^{5/2}) = Q/(1110D)^{5/2}$
R	Fire plume radius based on Gaussian radial distribution (m)
R_{fl}	Fire plume radius in flame zone (m)
s	Stoichiometric air/fuel ratio $= 15\cdot6$ (propane)
T_a	Ambient temperature of the highbay (K)
T_f	Film temperature (K)
T_{fl}	Flame temperature (K)

T_g	Compartment true gas temperature (K)
T_{gl}	Compartment lower-layer average true gas temperature (K)
T_{gu}	Compartment upper-layer average true gas temperature (K)
T_v	Compartment vent true gas temperature (K)
T_w	Compartment wall interior surface temperature (K)
T_{wl}	Compartment lower-layer average wall interior surface temperature (K)
T_{wu}	Compartment upper-layer average wall interior surface temperature (K)
T_∞	Surrounding temperature (K)
ΔT_g	Layer temperature difference between gas and wall $= \lvert T_{gu} - T_{wu} \rvert = \lvert T_{gi} - T_w \rvert$ (K)
U^*	Non-dimensional centerline velocity
w_c	Compartment width (m)
w_{fl}	Flame width at interface (m)
w_v	Vent width (m)
z	Elevation in compartment above floor (m)
z_b	Vent sill elevation (m)
z_{bl}	Boundary layer length $= z_i$ (lower layer) $= H - z_i$ (upper layer) (m)
z_i	Interface elevation, boundary between upper (hot) layer and lower (cold) layer (m)
z_n	Vent neutral plane elevation (m)
z_t	Vent soffit elevation (m)
z^*	Non-dimensional elevation $= z/D^*$
z_e^*	Non-dimensional entrainment height $= Z_i/D^*$
Z_e	Entrainment height $= z_i - 0 \cdot 61$ (m)
Z_{fl}	Mean flame height (50% intermittency) $= 0 \cdot 5(Z_{0 \cdot 0} + Z_{1 \cdot 0})$ (m)
Z_n	Near-field entrainment height offset (m)
Z_o	Far-field entrainment height offset (m)
$Z_{0 \cdot 0}$	0% intermittency flame height (m)
$Z_{1 \cdot 0}$	100% intermittency flame height (m)

Greek symbols

χ	Normalized flame intermittency $= (Z_{0 \cdot 0} - Z_{1 \cdot 0})/Z_{fl}$
ϕ	Equivalence ratio $= m_e/(sm_p)$
ϕ_{ft}	Flame tip equivalence ratio

γ	Constant for flame height correlation
η	Radiant fraction $= 0\cdot30$ (used for propane)
μ	Absolute viscosity (kg/m s)
ν	Kinematic viscosity (m²/s)
$\theta*$	Non-dimensional centerline temperature
ρ	Density (kg/m³)
ρ_a	Ambient density in highbay (kg/m³)
ρ_{fl}	Flame density (kg/m³)
ρ_{gl}	Compartment lower-layer average density (kg/m³)
ρ_{gu}	Compartment upper-layer average density(kg/m³)
ρ_∞	Surrounding density (kg/m³)

1 INTRODUCTION

When compartment fire models such as CFAST[1,2] are used for large fires in small compartments, all the oxygen entrainment occurs in the flame zone, since the hot layer interface quickly descends to near the fuel surface. A widely accepted consensus on an entrainment model which is valid down to the fuel surface does not yet exist. A review of existing models[3–9] shows that they are based primarily on data from smaller fires. Full-scale experiments are needed to complement the small- and medium-scale experiments[4,10–15] and limited full-scale experiments[16] that have been conducted to date.

To obtain further information on entrainment rates in the near field, i.e. below the mean flame height, 20 experiments were conducted in a compartment which is similar in size, geometry and construction to the standard fire test compartment.[17] A $0\cdot61\,\text{m} \times 1\cdot22\,\text{m}$ porous surface propane fired burner was used to give a full-scale size to the fires. The fires ranged from 330 to 980 kW, covering the range of full-scale fire heat release rates for this compartment from pre-flashover to beyond flashover. Compartment flashover is defined as an upper layer temperature in the compartment above 500°C.[18,19]

A two-layer environment[20,21] is produced inside a fire compartment. The layers are stably stratified, so little mass crosses the interface except in the region of the fire plume. The stable stratification isolates the lower layer, where mass flows towards the plume at relatively low velocities and ameliorates any elliptic flow field effect of the compartment. The entrainment process of the fire plume acts as a 'pump' to transfer mass from the lower layer into the upper layer. For a fire in a compartment, the height over which the fire entrains mass is from the

base of the fire to the hot/cold layer interface. A large fire readily allows measurement of near-field entrainment rates because the quasi-steady location of the hot/cold layer interface falls below the mean flame height. Once in the upper layer the mass either recirculates or exits the compartment through a vent.

Here, the near-field fire entrainment rates were determined by measuring vent gas, and compartment gas and wall temperature profiles in the quasi-steady state for each experiment as described by Quintiere et al.[22] Flame height (at 0 and 100% intermittency) and flame width measurements were also made. For $Q > 700$ kW, where the 0% intermittency flame height could not be measured, mean flame heights were calculated by extrapolating a curve fit of normalized flame intermittency, χ, for $330 < Q < 680$ kW. Comparisons between the entrainment data developed here and the literature are explored. Near-field curve fits modifying Zukoski's far-field model[3,4] are developed. An alternative model based on Thomas,[23] with an offset[3] for near-field entrainment is also explored. Comparisons between existing comprehensive entrainment models[4–8] and the data developed here are also studied. The model of Baum and McCaffrey[6] gives the best match to the data.

2 EXPERIMENTAL APPARATUS

The experiments were conducted in a fire test compartment which is $2\cdot5$ m $\times$ $3\cdot7$ m in plan and $2\cdot5$ m in height, see Fig. 1. The compartment has a single doorway, $0\cdot76$ m wide $\times$ $2\cdot0$ m high. The interior wall and ceiling surfaces are covered with stainless sheet steel (thickness $0\cdot8$ mm) which has an industrial heat-resistant coating. The walls behind the sheet steel are 25 mm of ceramic fiberboard backed by 16 mm of gypsum wallboard and 13 mm of plywood. The ceiling behind the sheet steel is 25 mm of ceramic fiberboard backed by 28 mm of gypsum wallboard and 13 mm of plywood. The floor is 25 mm of gypsum wallboard backed by 19 mm of plywood. The walls and ceiling of the compartment are supported by a steel stud frame that is tied into the floor plywood. The floor of the compartment is supported by a wooden frame which is elevated approximately 1 m above the floor of the highbay which contains the compartment. The highbay, $8\cdot9$ m $\times$ $6\cdot4$ m in plan and $6\cdot7$ m in height, provides a sheltered indoor environment around the compartment. In the highbay, outside the compartment, directly above the doorway is a $3\cdot0$ m square exhaust hood used to capture all the products of combustion produced in each experiment.

Burner Configuration Compartment Center
Burner 0.61m x 1.22 m
Burner Height 0.61m

Compartment
2.5m x 3.7m x 2.5m
Doorway 0.76m x 2.0m

Wall Cut Away

Left Wall

Corner Wall TCs
Depth 3.8mm, Spacing 0.15m

Aspirated TCs, Heights 0.15m,
0.75m, 1.20m, 1.65m, 2.25m

Corner Bare Bead TC Tree, Spacing 0.15m

Front Wall

Doorway Bare Bead
Thermocouple (TC) Tree
0.15m Spacing
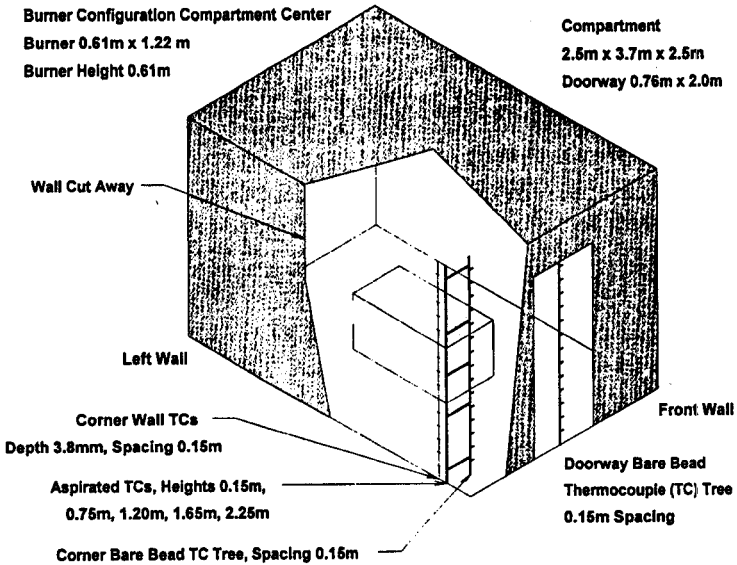
Fig. 1. Fire test compartment schematic showing burner configuration location and compartment instrumentation.

The exhaust system is instrumented[17] so that the heat release rate of a fire in the compartment can be determined by oxygen consumption calorimetry.[24]

The instrumentation in the compartment used to determine mass flow rates consists of a bare bead thermocouple tree in the doorway, a bare bead thermocouple and an aspirated thermocouple tree in the front left corner, and a vertical line of wall thermocouples in the front left corner, see Fig. 1. The doorway thermocouples are Type K 24 gauge (bead diameter 2 mm). The beads run along the doorway's vertical centerline in the vertical interior plane of the doorway frame. The beads are spaced at 0·15 m starting at 0·15 m above the floor and ending 1·95 m above the floor. The compartment corner bare bead thermocouples are also Type K 24 gauge. The beads were 0·30 m from both the front and left walls of the compartment. The beads were spaced at 0·15 m starting at 0·15 m above the floor and ending 2·25 m above the floor. The aspirated thermocouple probes were fabricated and operated to specifications given by Newman and Croce.[25] The probe shield intake ends were located 0·30 m from the left wall of the compartment and 0·25 m from the front wall. The probe heights above the floor were 0·15, 0·75, 1·20, 1·65 and 2·25 m. The wall thermocouples were Type K 30 gauge (bead diameter 1 mm). The beads were placed 3·8 mm beneath the

wall interior surface in the ceramic fiberboard. The beads ran along a vertical line in the left wall of the compartment, 0·41 m from the front wall. The beads were spaced at 0·15 m starting at 0·15 m above the floor and ending 2·25 m above the floor.

Four 0·30 m × 0·61 m porous surface burners were fabricated. The four burners were arranged in a 0·61 m × 1·22 m porous surface configuration with the porous surface 0·61 m above the floor of the compartment, see Fig. 1. The 0·61 m × 1·22 m burner was placed in the compartment at two locations: (1) centered front-to-back and left-to-right; and (2) centered front-to-back and against the right wall of the compartment. No difference could be detected in the experimental results in the two locations. The burners were propane fired and supplied at between 330 and 980 kW by a vaporizer/liquid tank system. The mass flow rate of propane was measured by using an orifice flange/plate built into the supply.[26–29]

3 EXPERIMENTAL PROCEDURES AND DATA REDUCTION

For each experiment, a burner configuration location in the compartment and heat release rate level were selected, see Table 1. The burner heat release rate was limited to avoid the production of significant flames out of the doorway of the compartment. The burner was supplied with propane at a steady state rate for the duration of the experiment. Each experiment was terminated when the compartment wall interior surface temperature was felt to have reached a quasi-steady state, see Table 1 for durations. Wall temperatures 3·8 mm beneath the wall interior surface and true gas temperatures at two elevations in the compartment are shown for a typical experiment in Fig. 2. The experiment shown is NAD-D004, where the heat release rate was 500 kW. The steady state supply rate of propane to the burner was stabilized at 7 min. The experiment was terminated at 37 min. The 30 min duration of the experiment was sufficient for the wall thermocouples to reach a quasi-steady state where the rate of change of the wall temperature was 3°C per min and decreasing.

For each experiment, the time averaged oxygen consumption heat release rate of the fire, Q_{O2}, and the time averaged potential heat release rate of the propane supplied to the burners, Q_p, were measured, see Table 1. As a check of the two values, the ratio Q_{O2}/Q_p was calculated for each experiment. From Table 1, it can be seen that the ratio varies over the range 0·94–1·06, with an average value of 0·99. This value is similar to that found by Tewarson.[30] For the heat release

TABLE 1

Duration, Burner Location and Heat Release Rate, and Vent Flow and Neutral Plane Elevation for Each Experiment (Data Listed by Increasing Q_{O2})

Experiment	Fire duration (min)	Burner configuration location	Q_{O2} (kW)	Q_P (kW)	Q_{O2}/Q_P	m_P (g/s)	m_i (kg/s)	m_o (kg/s)	m_i/m_o	z_n	m_{av} (kg/s)
NAD-D003	30	Center	330	330	1·00	7·1	0·85	0·89	0·95	1·04	0·87
NAD-D009	45	Side-wall	340	340	1·00	7·3	0·92	0·92	0·99	1·02	0·92
NAD-D013	43	Side-wall	370	350	1·06	7·5	0·93	0·90	1·04	1·04	0·92
NAD-D002	60	Center	430	420	1·02	9·1	0·97	0·94	1·04	1·02	0·96
NAD-D001	60	Center	450	420	1·07	9·1	0·98	0·94	1·05	1·02	0·96
NAD-D019	35	Side-wall	480	480	1·00	10·3	0·99	0·96	1·03	1·00	0·97
NAD-D014	33	Side-wall	480	500	0·96	10·8	0·99	0·96	1·04	1·00	0·98
NAD-D010	40	Side-wall	490	490	1·00	10·6	0·97	0·99	0·98	0·96	0·98
NAD-D004	30	Center	500	500	1·00	10·8	0·95	0·94	1·01	1·00	0·95
NAD-D020	30	Side-wall	620	660	0·94	14·2	0·99	1·02	0·97	0·94	1·00
NAD-D015	30	Side-wall	630	660	0·95	14·2	1·00	1·04	0·96	0·94	1·02
NAD-D007	35	Center	630	610	1·03	13·1	1·04	1·02	1·02	0·94	1·03
NAD-D011	33	Side-wall	630	660	0·95	14·2	1·06	1·03	1·03	0·94	1·05
NAD-D005	30	Center	680	670	1·01	14·4	1·02	0·98	1·04	0·96	1·00
NAD-D018	25	Side-wall	740	780	0·95	16·8	1·02	1·05	0·97	0·92	1·04
NAD-D016	25	Side-wall	770	790	0·97	17·0	1·03	1·04	0·99	0·92	1·04
NAD-D012	25	Side-wall	810	830	0·98	17·9	1·09	1·04	1·05	0·92	1·07
NAD-D008	25	Center	860	850	1·01	18·3	1·06	1·06	1·00	0·90	1·06
NAD-D017	20	Side-wall	900	940	0·96	20·3	1·05	1·07	0·98	0·90	1·06
NAD-D006	20	Center	980	930	1·05	20·0	1·03	0·99	1·04	0·92	1·01
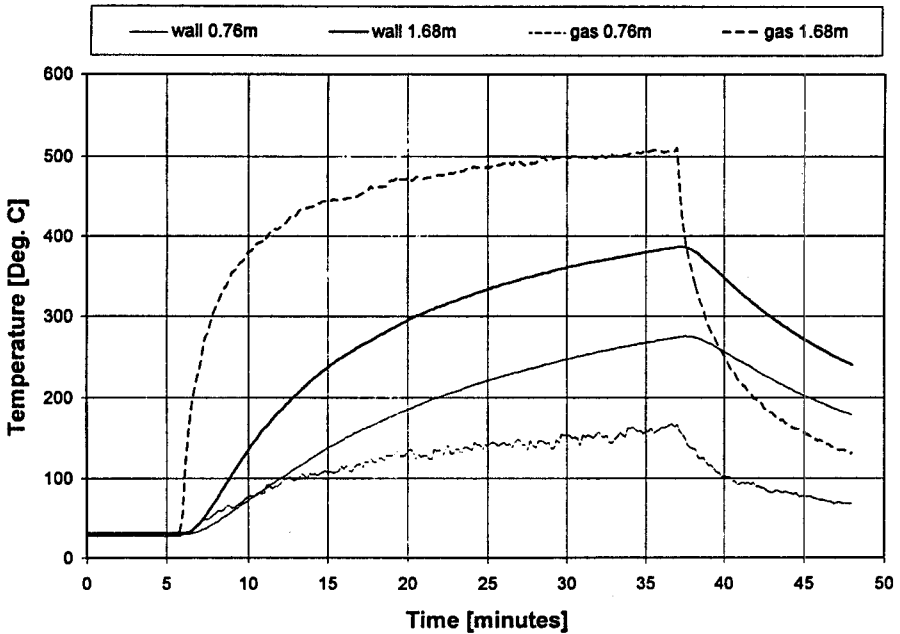
Fig. 2. Typical histories of compartment wall temperatures 3·8 mm beneath the wall interior surface and compartment true gas temperatures at two elevations. Experiment NAD-D004 is shown, heat release rate 500 kW.

rate levels used in these experiments, which are well below the ventilation-controlled[31] heat release rate for the compartment, $Q_{vc} = 1·6A_v h_v^{1/2} = 3·4$ MW, it would be expected that the propane would burn at maximum efficiency, $Q_{O2}/Q_p = 1$. The range of the ratio indicates that for these experiments, both the Q_{O2} and Q_p values determined are reasonable. When referring to fire heat release rates for the experiments, the value Q_{O2} will be used from this point forward.

For each experiment, all the measured quasi-steady state temperatures, i.e. compartment, doorway and wall, were calculated from time averages over the last 2 min of the experiment. All the thermocouples used were Type K (chromel–alumel) with a tolerance of ±2·2°C over the temperature range 0–1250°C.

To correct the bare-bead compartment thermocouples for radiation, five aspirated thermocouple/bare bead thermocouple pairs were used to develop a temperature correction profile. In the lower layer within the compartment, the correction decreases the bare bead temperature in the range 80–200°C. In the upper layer, the correction increases the bare bead temperature in the range 5–20°C. A typical compartment
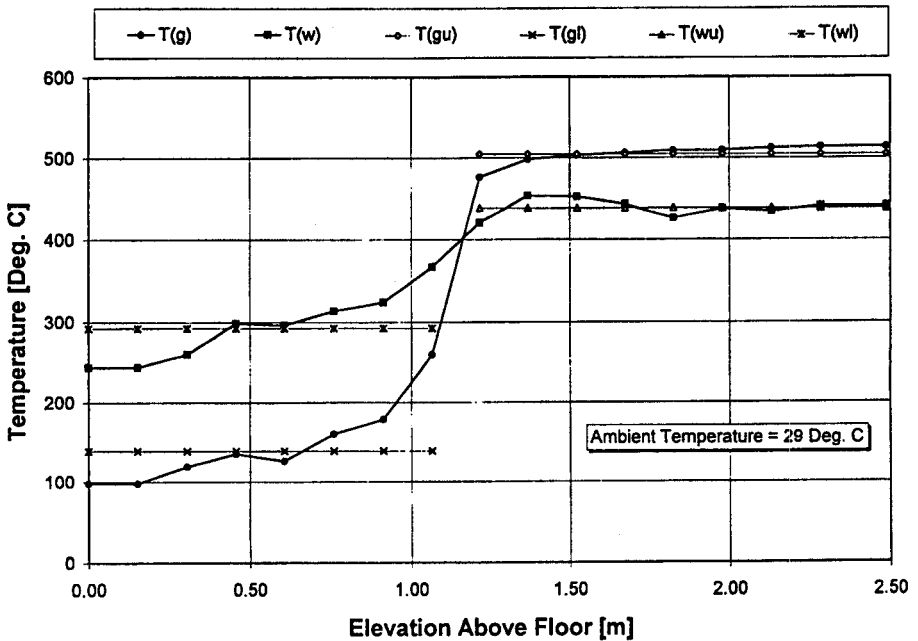
Fig. 3. Typical compartment steady-state gas true and quasi-steady state wall interior surface temperature profiles, and corresponding two-layer equivalents. Experiment NAD-D004 is shown, heat release rate 500 kW: (●), gas true temperature profile; (■), wall surface temperature profile.

gas steady-state true temperature profile is shown in Fig. 3. For this experiment, the doorway steady-state, bare-bead temperature profile is shown in Fig. 4.

Measuring a compartment gas true temperature profile (front corner), the doorway gas centerline temperature profile and a compartment wall surface temperature profile (front corner), see Fig. 1, allows the entrainment rate of a fire to be determined from the doorway vent flow, the doorway mixing, and the upward and downward boundary layer wall flows following the method of Quintiere et al.[22] This compartment method is analogous to the hood apparatus used by Cetegen et al.[4] to study entrainment of free-burning fires.

3.1 Vent mass flow rate

The compartment gas true temperature profile is used along with the doorway temperature profile to determine the doorway vent inflow and outflow. The method described below is similar to one used by
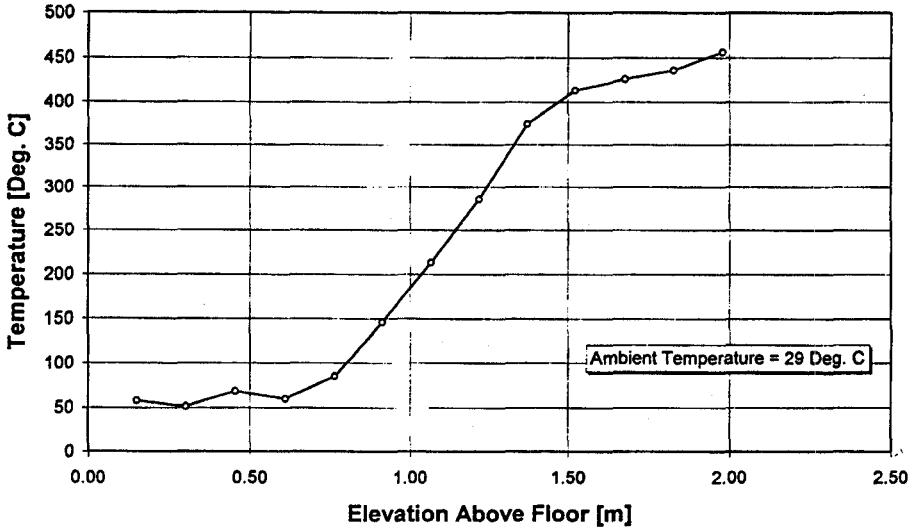
Fig. 4. Typical doorway steady-state bare-bead gas temperature profile. Experiment NAD-D004 is shown, heat release rate 500 kW.

Janssens and Tran.[32] The vent flow equations are derived by assuming hydrostatic pressure distributions in the compartment and ambient environment, and horizontal streamlines through the vent. The development of the equations is discussed in detail by others.[15,22,33,34] The equations are based on Emmons:[35]

$$m_o = C\rho_a T_a \sqrt{2g} \int_{z_n}^{z_t} w_v \left[\frac{1}{T_v} \int_{z_n}^{z} \left(\frac{1}{T_a} - \frac{1}{T_g} \right) dz' \right]^{1/2} dz \qquad (1)$$

$$m_i = C\rho_a T_a \sqrt{2g} \int_{z_b}^{z_n} w_v \left[\frac{1}{T_v} \int_{z}^{z_n} \left(\frac{1}{T_a} - \frac{1}{T_g} \right) dz' \right]^{1/2} dz \qquad (2)$$

For eqns (1) and (2), the ambient conditions are outside the compartment in the highbay. A single vent flow coefficient is used in eqns (1) and (2). Emmons[35] states: 'The best option now available is to use $C = 0.68$ and expect $\pm 10\%$ errors in flow calculations.'

Under steady state conditions, the vent mass outflow rate, m_o, is equal to the vent mass inflow rate, m_i, plus the propane mass flow rate, m_p, supplied to the burners. For these experiments, the mass flow rate of the propane is small as compared to the vent mass flows, see Table 1, and is neglected. For the steady state, $m_o = m_i$. With this condition, and eqns (1) and (2), the system can be solved iteratively for the doorway neutral plane elevation, z_n, which balances the vent mass flows. To

have the iterative solution converge to the correct vent mass flows, the effects of radiation on the doorway bare bead thermocouples must be accounted for. Below the neutral plane elevation, temperatures were set to ambient, and above the neutral plane elevation, the temperature correction profile used for the compartment thermocouples was applied.

The doorway neutral plane elevation was solved for to the nearest 20 mm for each experiment. These neutral plane locations resulted in vent mass flows of $0.95 < m_i/m_o < 1.05$, see Table 1. For the purpose of determining the experimental entrainment rate, the average, m_{av}, of m_o, and m_i will be used, see Table 1.

3.2 Equivalent two-layer gas environment and vent mixing

To determine the doorway vent mixing for these experiments, the gas temperature profiles need to be represented as two-layer equivalents. The following method[22] was used:

$$\int_0^H (T_g^{-1})\,dz = [H - z_i]T_{gu}^{-1} + z_i T_{gl}^{-1} \tag{3}$$

$$\int_0^H (T_g)\,dz = [H - z_i]T_{gu} + z_i T_{gl} \tag{4}$$

Equation (3) represents mass equivalence and eqn (4) maintains the average temperature. The two integral identities can be used to solve for the lower-layer average gas temperature, T_{gl}, and the interface elevation, z_i, if the upper-layer average gas temperature, T_{gu}, is determined from the profile directly. A typical compartment gas temperature two-layer equivalent is shown in Fig. 3. An examination of Fig. 3 shows that the calculated interface elevation is located to no more than ±80 mm. The calculated upper- and lower-layer average gas temperatures, and interface elevations for each experiment, are listed in Table 2.

For each experiment, it is found that $z_i > z_n$. An explanation for why $z_i > z_n$ may be found in the drop in elevation in the region immediately adjacent to the front wall, of the smoke traces left on the compartment walls by the upper layer. The flow that exists in the compartment near the doorway is very complex and three-dimensional.[10] It seems reasonable to assume that the drop in elevation of the smoke trace is due to these complex flow patterns. Review of experimental data[15] shows that

TABLE 2

Gas and Wall Interior Surface Two-layer Equivalent Temperatures and Interface Elevation, Wall Flow and Vent Mixing, and Entrainment Rate and Equivalence Ratio for Each Experiment (Data Listed by Increasing Q_{O2})

Experiment	Q_{O2} (kW)	T_{gu} (°C)	T_{gl} (°C)	Z_i (m)	T_{wu} (°C)	T_{wl} (°C)	m_{wu} (kg/s)	m_{wu}/m_{av}	m_m (kg/s)	m_m/m_{av}	m_e (kg/s)	m_e/m_p	ϕ
NAD-D003	330	370	84	1·12	315	187	0·17	0·19	0·033	038	0·74	104	6·6
NAD-D009	340	402	102	1·12	355	208	0·16	0·17	0·036	0·039	0·80	109	7·0
NAD-D013	370	417	94	1·12	366	217	0·17	0·18	0·031	0·034	0·78	103	6·6
NAD-D002	430	462	117	1·12	391	268	0·17	0·17	0·035	0·037	0·82	91	5·8
NAD-D001	450	472	120	1·12	386	265	0·17	0·17	0·035	0·036	0·83	92	5·9
NAD-D019	480	509	132	1·12	452	283	0·16	0·17	0·032	0·33	0·84	81	5·2
NAD-D014	480	507	134	1·12	452	283	0·16	0·17	0·028	0·029	0·84	78	5·0
NAD-D010	490	503	146	1·12	460	287	0·16	0·16	0·038	0·038	0·86	82	5·2
NAD-D004	500	505	138	1·12	439	292	0·16	0·17	0·035	0·037	0·82	76	4·9
NAD-D020	620	608	168	0·99	549	347	0·14	0·14	0·044	0·044	0·91	64	4·1
NAD-D015	630	610	162	0·99	553	348	0·14	0·14	0·042	0·041	0·92	65	4·1
NAD-D007	630	610	179	1·04	566	342	0·14	0·14	0·041	0·039	0·93	70	4·5
NAD-D011	630	611	184	0·96	564	363	0·14	0·13	0·051	0·049	0·96	67	4·3
NAD-D005	680	639	162	0·99	580	410	0·15	0·15	0·039	0·039	0·89	62	3·9
NAD-D018	740	675	204	0·99	600	387	0·13	0·13	0·045	0·043	0·95	56	3·6
NAD-D016	770	696	205	0·99	626	410	0·14	0·13	0·041	0·040	0·94	55	3·5
NAD-D012	810	710	240	0·96	654	442	0·13	0·12	0·049	0·046	0·98	55	3·5
NAD-D008	860	750	255	0·96	713	467	0·13	0·12	0·049	0·046	0·98	54	3·4
NAD-D017	900	759	245	0·96	679	435	0·13	0·12	0·043	0·040	0·98	48	3·1
NAD-D006	980	796	236	0·99	728	471	0·14	0·13	0·035	0·034	0·91	45	2·9

36 out of 55 experiments conducted had $z_i > z_n$. The vent flow coefficients[15] determined fall within the bounds of $C = 0.68 \pm 10\%$ for various doorway and window configurations. It seems likely then that the drop in elevation is incorporated within the value of the vent flow coefficient used here.

Lim's model[10] can be used to estimate the doorway vent mixing for each experiment. Lim assumes that fresh air enters the room like a turbulent wall jet with a mixing layer separating the upper (hot) and lower (cold) layers. Fixing is from the upper layer into the lower layer. The model[10] is:

$$\left[\frac{1}{2}\left(\frac{m_m}{m_{av}}\right)^2 + \frac{m_m}{m_{av}}\right]\left[1 + \frac{m_m}{m_{av}}\right]^2 = 11.7F^2 \tag{5}$$

where

$$F = \frac{\rho_{gu}w_v}{\rho_a w_c}\frac{1}{\sqrt{Ri}}$$

$$Ri = \frac{\Delta\rho g z_i}{\rho_a U_c^2}$$

$$\frac{\Delta\rho}{\rho_a} = \frac{T_a}{T_{gl}} - \frac{T_a}{T_{gu}}$$

and

$$U_c = \frac{m_{av}}{\rho_a w_v z_i}$$

The vent mixing mass flow rates, m, are, on average, 4% of m_{av}, see Table 2.

3.3 Wall mass flow rates

To estimate the wall flows that occur in the compartment, Jaluria's method[36] was used. The method assumes steady-state, two-dimensional, natural convective boundary layer flows with isothermal vertical surfaces and isothermal quiescent environments. To use this method, the two-layer equivalents for both the gas temperature and the wall interior surface temperature are required.

The wall surface temperatures were estimated from the wall temperatures 3.8 mm beneath the wall interior surface by using the solution for the temperature in a semi-infinite solid with a constant

heat flux boundary condition.[37] The thermal properties of the ceramic fiberboard were used: conductivity $= 0.10$ W/m K, density $= 449$ kg/m³ and specific heat $= 1090$ J/kg K. A typical wall interior surface temperature profile is shown in Fig. 3.

The two-layer equivalents for the wall interior surface temperatures for each experiment were determined using z_i, calculated from the gas two-layer equivalents. The interface elevations along with the average upper-layer wall interior surface temperatures, T_{wu}, taken directly from the profiles, allow one of the integral identities, eqn (3) or eqn (4), to be used to calculate the average lower-layer wall interior surface temperatures, T_{wl}, see Table 2. A typical wall interior surface two-layer equivalent is shown in Fig. 3.

Review of the temperature profiles and the two-layer equivalents in Fig. 3, and the average layer temperatures listed in Table 2 shows that the lower-layer wall surface temperature is greater than the gas temperature. This will result in an upward boundary layer flow along the compartment wall. For the upper layer, the situation is reversed. The momentum of these two flows at the interface controls whether there is a net upward or downward flow.[36]

The boundary layer momentum and mass-flow rate at the interface for both upward and downward flow was calculated. The gas properties used were for air at the film temperature for each layer. The boundary layer length at the interface, z_{bl}, for upward flow is $z_{bl} = z_i$ and for downward flow is $z_{bl} = H - z_i$. The Grashof number, Gr, for each layer is:

$$Gr = g\Delta T z^3_{bl}/(T_f v^2) \tag{6}$$

where $z_{bl} = z_i$ or $z_{bl} = H - z_i$. The momentum per unit width for each layer is taken as:

$$M = 0.5\rho v^2(0.802 Gr^{3/4} + 0.036 Gr^{9/10})/z_{bl} \tag{7}$$

The wall mass flow rate per unit width for each layer is taken as:

$$m_w = 0.5\mu(1.755 Gr^{1/4} + 0.101 Gr^{2/5}) \tag{8}$$

To get the actual wall mass flow rate, the flow rate per unit width is multiplied by the solid wall perimeter of the compartment.

For all the experiments, the ratio of upward momentum to downward momentum was in the range $1.9-3.8$, with an average value of 2.6. The upward momentum was considered sufficiently larger than the downward momentum to cause a net upflow across the interface of the entire lower-layer wall flow.[36] The calculated lower-layer upflows m_{wu}, are, on average, 15% of m_{av}, see Table 2.

3.4 Near-field entrainment rate, and flame height and width

The entrainment mass flow rate of each experiment, m_e, was determined as:

$$m_e = m_{av} + m_m - m_{wu} \tag{9}$$

The mass flow rate of the propane is small compared to m_e in each experiment, and is neglected. This means that the entrainment mass flow rate is the same as the plume mass flow rate. For these experiments, the entrainment rates determined are essentially the doorway average vent mass flow rates. This is because the doorway mixing and the wall flows only decrease the average vent flow rate by approximately 10%. For these compartment fires, the height over which the fires entrain mass is from the base of the fire to the hot/cold layer interface which includes any mass that crosses the horizontal plane at the base of the fire.

It is found in these experiments that the fire entrainment rates increase, at a decreasing rate, with increasing fire heat release rate and range from 0·74 to 0·98 kg/s, see Fig. 5 and Table 2. The position of
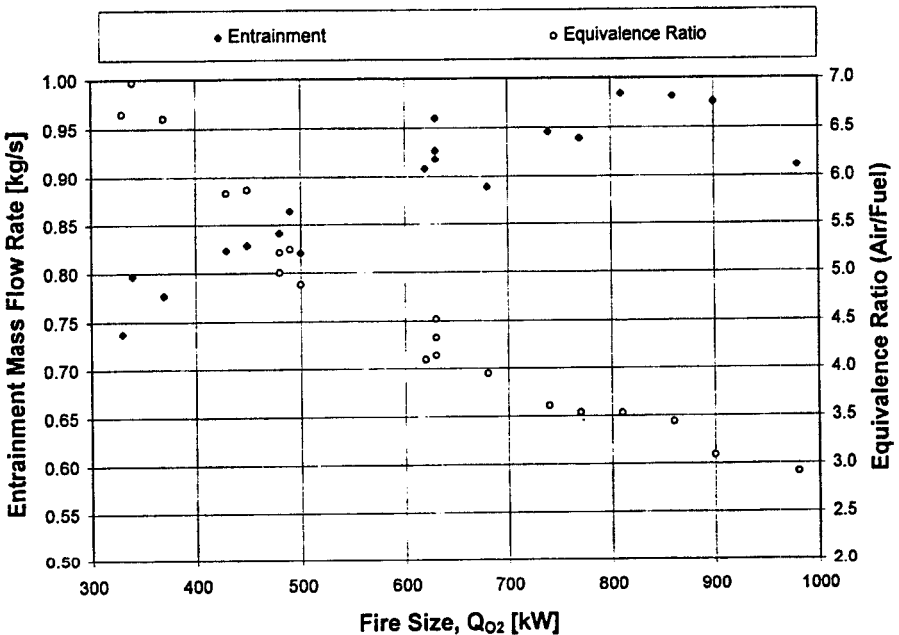
Fig. 5.   Experimental entrainment rates and equivalence ratios vs fire size.

the burner configuration did not affect the entrainment rates. The equivalence ratio (air/fuel), σ, ranges from 7·0 to 2·9, see Fig. 5 and Table 2. The overventilated (fuel lean) equivalence ratios are consistent with the fact that the fire heat release rates used in these experiments are well below the ventilation controlled rate of 3·4 MW.

The exact error bounds on the various components of the entrainment calculation are not sufficiently well known to justify a detailed error analysis. The entrainment rates determined are considered to have an accuracy of ±20%.

A video tape and still photograph record was made of each experiment. Review of portions of the video tape (frame by frame) and of the photographs allowed the mean flame height and flame width at the interface for each experiment to be determined. The flames, as they rise above the burner configuration surface, neck-in along both the long and short sides of the burners such that as the flames rise they are converging to a cylindrical shape. The necking-in of the flames is such that at the interface, an approximate cylindrical shape exists so that the flame width at the interface can be considered analogous to the diameter of the flame plume. Although the flames wander in all the experiments, on a time average, the flames are basically vertical, unlike the blown over plumes observed for small fires.[15] The flames for the side-wall configuration do not appear to be significantly affected by the presence of the right-hand wall of the compartment. This is consistent with the above discussion, where the entrainment rates of the experiments were not affected by the location of the burners.

The mean flame height was defined as suggested by Zukoski.[4] From the video tape, the 0% intermittency flame height, $Z_{0\cdot0}$, and the 100% intermittency flame height, $Z_{1\cdot0}$, were measured. It was found that for the experiments where $Q_{O2} > 700$ kW, $Z_{0\cdot0}$ could not be measured reliably due to the interaction between the compartment ceiling and the flames. For the experiments where a reliable $Z_{0\cdot0}$ exists, the mean flame height (50% intermittency), Z_{fl}, was calculated as:

$$z_{fl} = 0\cdot5(Z_{0\cdot0} + Z_{1\cdot0}) \tag{10}$$

To determine Z_{fl} for the remaining experiments the quantity $\chi = (Z_{0\cdot0} - Z_{1\cdot0})/Z_{fl}$ was calculated from the experiments which have a reliable $Z_{0\cdot0}$ value. The quantity χ was fitted to a curve over the range $330 < Q_{O2} < 680$ kW as $\chi = 9\cdot4Q_{O2}^{-0\cdot42}$. This fit was used to estimate χ for $Q_{O2} > 700$ kW. With χ and $Z_{1\cdot0}$ known, Z_{fl} can easily be solved for:

$$Z_{fl} = Z_{1\cdot0}/(1 - 0\cdot5\chi) \tag{11}$$

The mean flame height, χ and the flame width at the interface are

TABLE 3
Mean Flame Height, Normalized Flame Intermittency, Flame Width at the Interface, Entrainment Height, Normalized Entrainment Height, Model[6] Plume Radius and Normalized Flame Width for Each Experiment (Data Listed by Increasing Q_{O2})

Experiment	Q_{O2} (kW)	Z_{fl} (m)	χ	W_{fl} (m)	Z_e (m)	Z_e/Z_{fl}	z_e^*	R (m)	$0.5w_{fl}/R$
NAD-D003	330	0·60	0·84	0·3	0·51	0·85	0·82	0·27	0·55
NAD-D009	340	0·65	0·86	0·4	0·51	0·78	0·81	0·28	0·73
NAD-D013	370	0·65	0·93	0·3	0·51	0·78	0·79	0·28	0·53
NAD-D002	430	0·75	0·64	0·4	0·51	0·68	0·74	0·30	0·66
NAD-D001	450	0·75	0·64	n/a	0·51	0·68	0·73	0·31	n/a
NAD-D019	480	0·50	0·69	0·5	0·51	0·64	0·71	0·31	0·80
NAD-D014	480	0·85	0·72	0·5	0·51	0·60	0·71	0·32	0·79
NAD-D010	490	0·75	0·72	0·5	0·51	0·68	0·71	0·32	0·79
NAD-D004	500	0·80	0·69	0·4	0·51	0·64	0·70	0·32	0·62
NAD-D020	620	1·05	0·55	0·5	0·38	0·36	0·48	0·35	0·72
NAD-D015	630	1·05	0·81	0·5	0·38	0·36	0·48	0·35	0·71
NAD-D007	630	0·90	0·67	0·5	0·43	0·48	0·54	0·35	0·71
NAD-D011	630	1·00	0·65	0·6	0·35	0·35	0·45	0·35	0·85
NAD-D005	680	1·00	0·62	0·6	0·38	0·38	0·46	0·36	0·8
NAD-D018	740	1·10	0·60	0·7	0·38	0·35	0·45	0·37	0·94
NAD-D016	770	1·10	0·59	0·7	0·38	0·35	0·44	0·38	0·92
NAD-D012	810	1·05	0·58	0·7	0·35	0·33	0·40	0·39	0·90
NAD-D008	860	1·05	0·56	0·6	0·35	0·33	0·39	0·40	0·76
NAD-D017	900	1·00	0·55	0·8	0·35	0·35	0·39	0·40	0·99
NAD-D006	980	1·05	0·53	0·6	0·38	0·36	0·40	0·42	0·72

shown in Table 3 for all the experiments. Comparisons with the flame height literature are discussed in the Appendix.

It is important to know the mean flame height for a fire because it can be used to define the boundary between the near-field fire plume and the far-field fire plume. The near field is below the mean flame height and the far field is above the mean flame height. In Table 3, the entrainment heights, Z_e, are listed for each experiment. They range in height from 0·35 to 0·51 m. The ratio Z_e/Z_{fl} was calculated for each experiment and is also shown in Table 3. For each experiment, the ratio is less than one indicating that all the entrainment rates determined are in the near-field.

4 COMPARISON OF RESULTS

4.1 Entrainment literature

Entrainment data from the literature [4,10–16] were compiled to form a data set of buoyancy-driven gas burner and pool fires that range in size

TABLE 4
Number of Data Points, and Fire Size and Flame Heights from the Literature Used in
Fig. 6 and eqn (13)

Literature data source	Number of data points in Fig. 6	Number of points used in eqn (13)	D (m)	Q (kW)	Z_{fl} based on
Cetegen et al.[4]	365	359	0·10, 0·19, 0·30, 0·50	3–158	Cetegen et al.[4]
Lim[10]	14	3	0·19	11–126	Cetegen et al.[4]
Toner et al.[11]	11	2	0·19	12–136	Cetegen et al.[4]
Morehart et al.[12]	2	0	0·19	31–68	Cetegen et al.[4]
Tokunaga et al.[13]	35	35	0·23, 0·30, 0·50	21–82	Cetegen et al.[4]
Yumoto and Koseki[14]	3	2	0·30	90	Cetegen et al.[4]
Thomas et al.[16]	8	6	0·91	509	Measurement
Steckler et al.[15]	55	18*	0·30	32–158	Cetegen et al.[4]
Dembsey	20	20	0·81	330–980	Measurement

* Only burner compartment side-wall included. Burner compartment center entrainment increased
due to wind effect. Burner compartment corner entrainment decreased due to wall effect.

of hydraulic diameter from 0·10 to 0·91 m and heat release rate from 3
to 980 kW, see Table 4. Entrainment measurements for this data set
were taken at various elevations above the burner/pool surface from
near 0% of the mean flame height to just over 500% of the mean flame
height. For the data set, plume mass flow rates and entrainment mass
flow rates are considered identical. This data set can be correlated using
a far-field entrainment model with virtual origin,[4] see eqn (12), and Figs
6 and 7, where the measured entrainment rates are normalized on the
far-field entrainment rate. For each data point, the mean flame height
was based on a correlation[4] or on flame height measurements, see Table
4. The use of actual flame height measurements is important for the
data of Thomas et al.[16] and the results developed here because the
measured flame heights do not match the following correlation.

$$m_f = 0·21\rho_\infty\sqrt{g Z_v}\, Z_v^2 Q_{zv}^{*1/3} \tag{12}$$

where $Z_v = Z_e + Z_o$; $Q_{zv}^* = Q/(\rho_\infty c_p T_\infty \sqrt{g} Z_v^{5/2}) = Q/(1110 Z_v^{5/2})$ and with
the floor $Z_o/D = 0·50 - 0·33 Z_{fl}/D$, without the floor $Z_o/D = 0·80 -
0·33 Z_{fl}/D$; $Z_{fl}/D = 3·3 Q_D^{*n}$; and for $Q_D^* < 1$, $n = 2/3$ while for $Q_D^* > 1$,
$n = 2/5$.

A curve fit of the data was developed and is shown in eqn (13), and
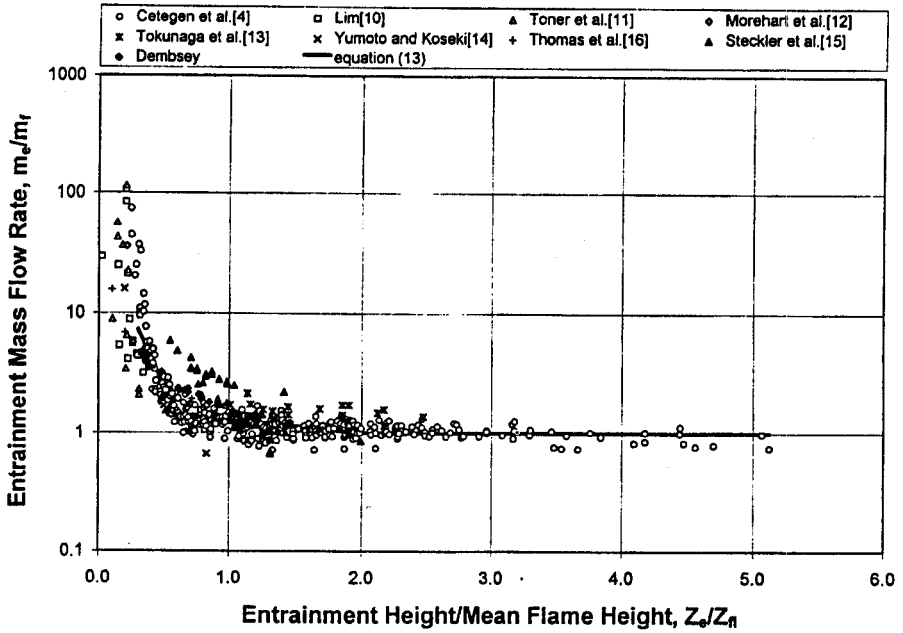
Fig. 6. Compiled entrainment rate data and curve fit. Entrainment rate normalized by far-field model and entrainment height normalized by mean flame height.

Figs 6 and 7. It should be noted that 81% of the data points used in the curve fit are from Cetegen *et al.*[4] see Table 4.

$$m = \beta m_{\mathrm{f}} \qquad (13)$$

where $\beta = 1$ for $Z_e/Z_{fl} \geq 2$; $\beta = \exp(0 \cdot 52 - 0 \cdot 26 Z_e/Z_{fl})$ for $0 \cdot 6 \leq Z_e/Z_{fl} \leq 2$; and $\beta = 1 \cdot 4 \exp(3 \cdot 2 - 5 \cdot 4 Z_e/Z_{fl})$ for $0 \cdot 3 \leq Z_e/Z_{fl} \leq 0 \cdot 6$.

The factor β is expected to be equal to unity for $Z_e > 2Z_{fl}$ since the far-field solution should be valid at $2Z_{fl}$. The range of Z_e from $2Z_{fl}$ down to $0 \cdot 6 Z_{fl}$ shows β increasing nearly linearly to a value of $1 \cdot 4$. Below $0 \cdot 6 Z_{fl}$, β increases much more quickly. Below $0.3Z_{fl}$, the data scatter significantly and were not included in the curve fit, see Table 4. It is interesting that the rapid increase in β beyond $1 \cdot 4$ corresponds to $0 \cdot 6 Z_{fl}$. For the experiments conducted here and for the $0 \cdot 50$ m diameter burner data from Cetegen *et al.*,[4] $0 \cdot 6 Z_{fl}$ is roughly the 100% intermittency flame height. The experiments conducted here have an average value of $\chi = 0 \cdot 67$ which gives $Z_{1 \cdot 0} = 0 \cdot 66 Z_{fl}$. Similarly the $0 \cdot 50$ m diameter burner data from Cetegen *et al.* have an average value of $\chi = 0 \cdot 75$ which gives $Z_{1 \cdot 0} = 0 \cdot 62 Z_{fl}$.

The data used in the curve fit show that the data for diameters less than or equal to $0 \cdot 50$ m do not necessarily correspond to the same
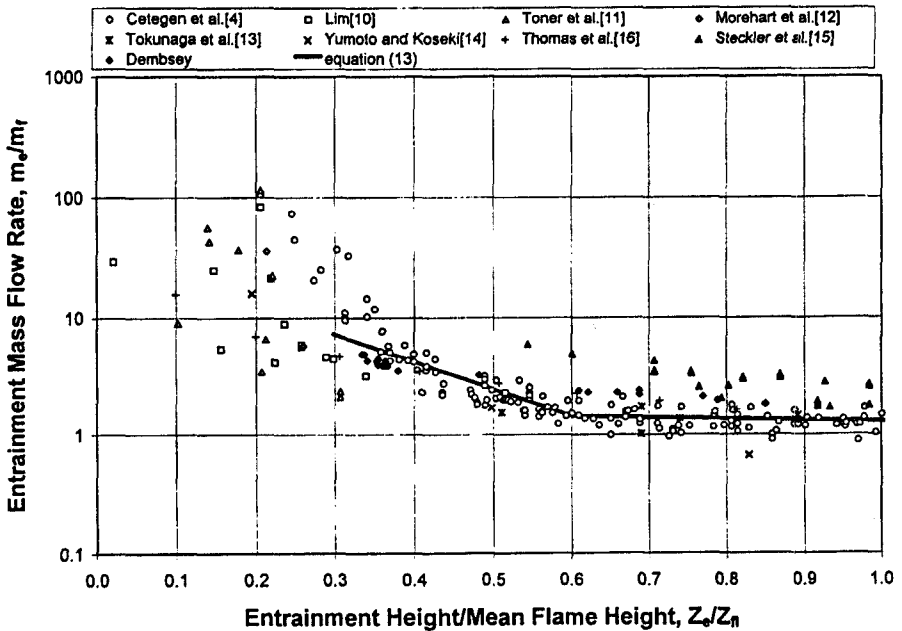
Fig. 7. Compiled entrainment rate data and curve fit, abscissa 0·0–1·0. Entrainment rate normalized by far-field model[4] and entrainment height normalized by mean flame height.

curve fit as for data for diameters greater than 0·50 m, see Fig. 7. An alternative curve fit for diameters greater than 0·50 m was also done based on the data generated here, see eqn (14) and Fig. 8.

$$m = \beta m_f \qquad (14)$$

where $\beta = 1\cdot3\exp(1\cdot8-1\cdot8Z_e/Z_{fl})$ for $0\cdot3 \leq Z_e/Z_{fl} < 1\cdot0$

The factor β in eqn (14) was matched to the factor β in eqn (13) at the mean flame height. From Fig. 8, it can be seen that eqn (14) does not show a change in behavior at $0\cdot6Z_{fl}$.

The importance of eqns (13) and (14) is that it appears that the variables D, Q, Z_e, Z_{fl} and ρ_∞ are sufficient to correlate the entrainment data of a wide range of fires as long as the actual mean flame heights are used. The actual flame heights provide a characteristic length scale that can account for other variables that are not explicit in eqns (13) and (14). How compartment and vent geometry, and fire elevation affect entrainment was not addressed in these experiments.

Near-field entrainment rates calculated from eqns (13) and (14) should be viewed as estimates only. This is because of the nature of the far-field model and its modification. As the entrainment height is
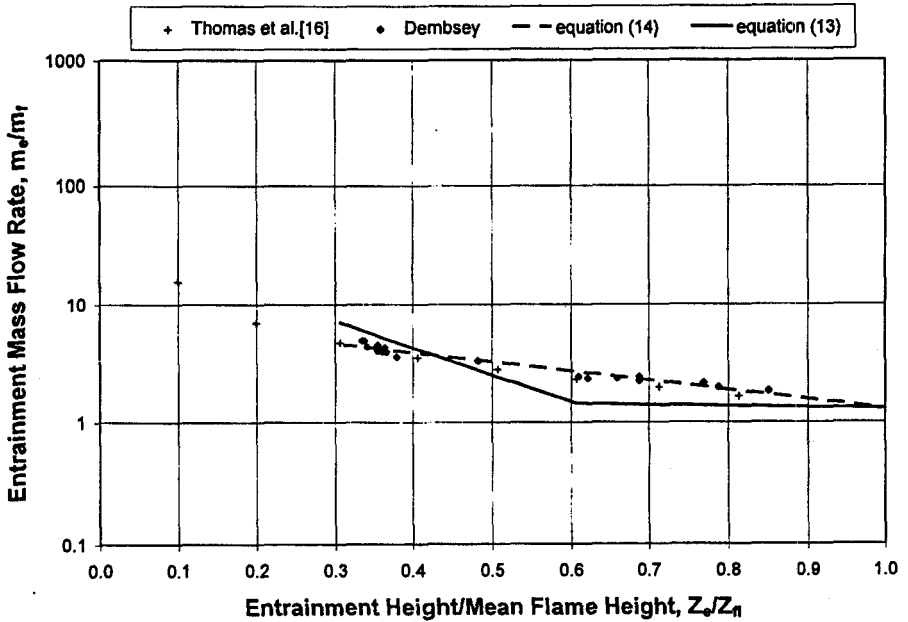
Fig. 8. Experimental entrainment rate data and curve fit, and data of Thomas *et al.*[16] Entrainment rate normalized by far-field model[4] and entrainment height normalized by mean flame height.

decreased, the far-field entrainment mass flow rate decreases and the modification increases to give the correct entrainment rate in the near field. For the far-field model, as the entrainment height decreases, the effect of the virtual origin on entrainment mass flow rate increases. The accuracy of the virtual origin is, therefore, very important in the lower half of the flame because the modification becomes large and will greatly magnify any error caused by the virtual origin. In the upper half of the flame and above, any error in the entrainment mass flow rate caused by the virtual origin is reduced due to the increased entrainment height. The far-field modification in the upper half of the flame and above is not large, so that any error caused by the virtual origin will not be greatly magnified. The near-field entrainment estimates of eqns (13) and (14) should be viewed as reasonable in the upper half of the flame and as questionable in the lower half of the flame.

4.2 The near-field model of Thomas

Another way to determine the near-field entrainment rate of a fire is to use the model of Thomas[23] as suggested by Zukoski.[3] The near-field portion of the data in the literature,[4,10–16] corresponding to $D \geq 0.19\,\text{m}$
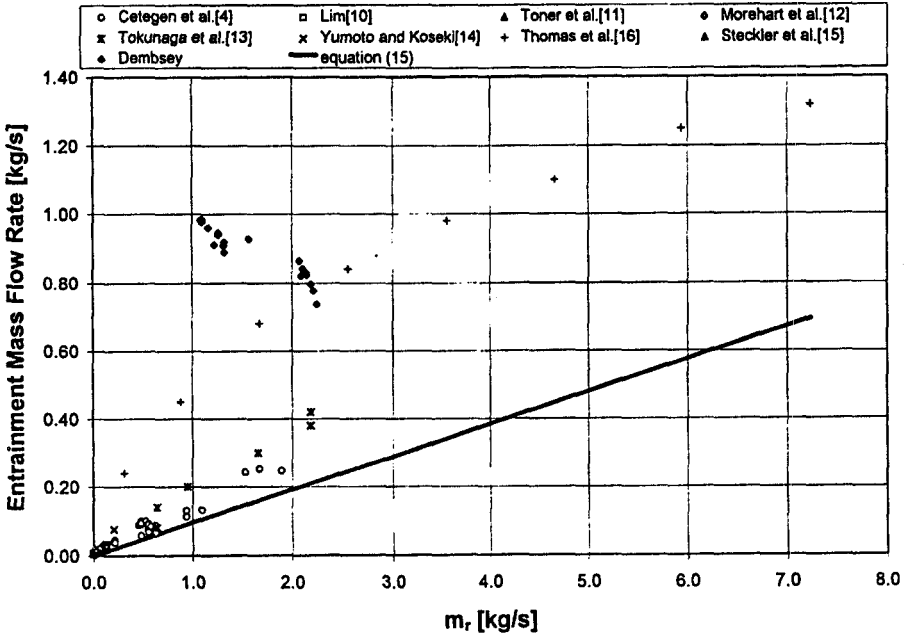
Fig. 9. Compiled near-field entrainment rate data and near-field model[23] vs reduced form of model.

was compared to the model[23] in eqn (15), see Fig. 9. The data for $D < 0.19$ m was not used because 68 out of 103 data points have $Q_D^* > 8$, which indicates a different flame regime[3]. The remaining 35 points were not used because of their more laminar flame structure.[3] Figure 9 shows that the model[23] does not represent the data very well.

$$m = 0.096 P Z_e^{3/2} (g\rho_\infty \rho_{fl})^{1/2} = 0.096 m_r \qquad (15)$$

where $\rho_{fl}\{T_{fl} = 1185\text{ K}\} = 0.298$ kg/s.

To match the model to the data, an offset to Z_e was calculated for each data point. For hydraulic diameters less than 0·50 m, the normalized offset was found to be of the order one, and not a function of Q_D^*, see eqn (16) and Fig. 10. This is similar to what Zukoski[3] found. The normalized offset for $D \geq 0.50$ m was found to be a linear function of Q_D^*, see eqn (16) and Fig. 10.

$$m = 0.096 P (Z_e + Z_{fl})^{3/2} (g\rho_\infty \rho_{fl})^{1/2} = 0.096 m_{ro} \qquad (16)$$

where $Z_{fl}/D = 1.3 Q_D^*$ for $D \geq 0.50$ m and $Z_{fl}/D = 0.9$ for $D \leq 0.50$ m.

The model[23] with offsets, eqn (16), is shown with data from the near-field literature[4,10–16] in Fig. 11. When compared to Fig. 9, Fig. 11
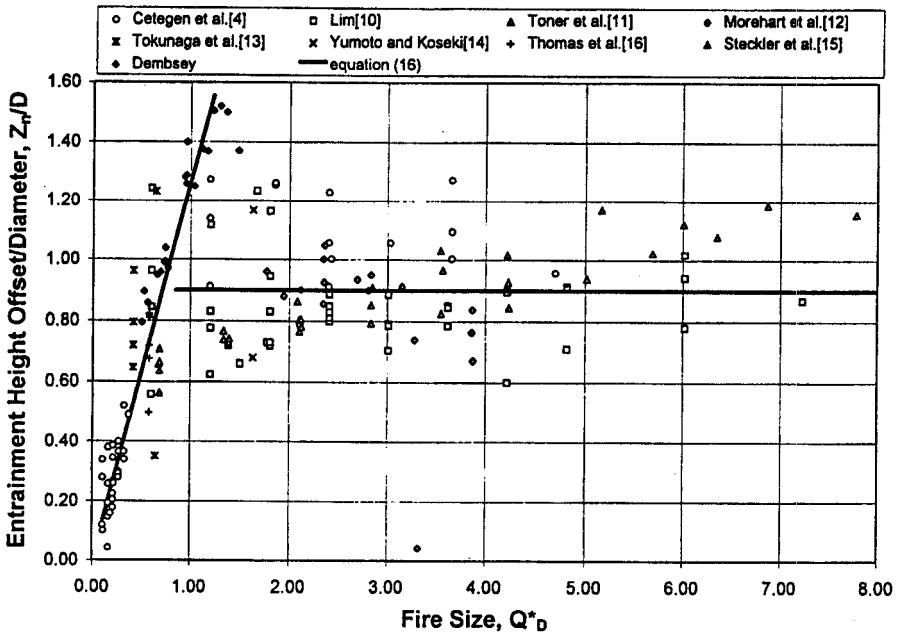
Fig. 10. Normalized near-field model[23] offset and offset curve fit versus normalized fire size.

demonstrates a significant improvement in the model by using an offset. Due to the limited data set developed here, the offset correlation of eqn (16) should be viewed as preliminary. For the burners with $D \geq 0.50\,\text{m}$, the near-field offset, Z_{fl} is a function of Q_D^*. The fact that the offset is a function of Q_D^* implies that the heat release rate of the fire influences the entrainment rate. This is contrary to the original form of Thomas'[23] model, eqn (15), where the only fire characteristics of importance are the perimeter and the flame temperature.

4.3 Fire plume models

The compartment fire environment conditions determined for each experiment, Tables 1, 2 and 3, were used as input data for the comprehensive models of McCaffrey,[5] Baum and McCaffrey,[5] Cetegen et al.,[4] Delichatsios[7] and Heskestad[8] to calculate entrainment rates for each of the experiments. The relevant parts of the models are shown in eqns (17)–(20) and for Baum and McCaffrey in eqns (21)–(25).
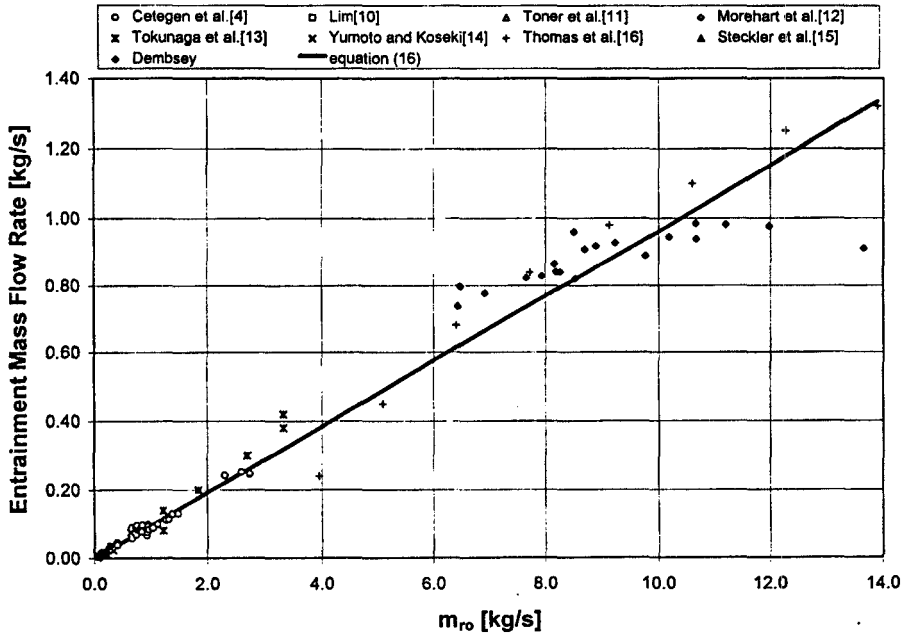
Fig. 11. Compiled near-field entrainment rate data and near-field model with offset vs reduced form of model with offset.

4.3.1 McCaffrey

$$m/Q = C_1\xi^q \qquad (17)$$

where $\xi = Z_e/Q^{2/5}$ and for $0 < \xi < 0.08$, $C_1 = 0.011$ and $q = 0.566$; for $0.08 < \xi < 0.20$, $C_1 = 0.026$, and $q = 0.909$; and for $0.20 < \xi$, $C_1 = 0.124$, and $q = 1.895$.

4.3.2 Cetegen et al.

$$m = m_1 = 0.447\rho_\infty D Z_e^{3/4} \qquad (18)$$

where for $Z_e \leq Z_{t2}$, $m = m_3 = m_f$; and for $Z_e > Z_{t2}$, $m_1\{Z_{t2}\} = m_3\{Z_{t2}\}$.

4.3.3 Delichatsios (near-field)

$$m = C_2(s + 1)m_p Fr^{-1}(Z_e/D)^r \qquad (19)$$

where for $Z_e/D < 1$, $C_2 = 0.086$, and $r = 1/2$; for $1 < Z_e/D < 5$, $C_2 = 0.093$, and $r = 3/2$; for $Z_e/D > 5$, $C_2 = 0.018$, and $r = 5/2$; and where

$$Fr = Q_D^*[(\Delta H_c[(s + 1)c_p T_\infty]^{-1})^{3/2}(1 - \eta)^{1/2}]^{-1}$$

4.3.4 *Heskestad*

$$m = 0.0054Q_cZ_e/(0.166Q_c^{2/5} + Z_o') \tag{20a}$$

for $Z_e \le Z_1$ and

$$m = 0.071Q_c^{1/3}(Z_e - Z_o')^{5/3}[1 + 0.026Q_c^{2/3}(Z_e - Z_o')^{-5/3}] \tag{20b}$$

for $Z_e > Z_1$, where $Z_1 = Z_o' + 0.166Q_c^{2/5}$ and $Z_o' = -1.02D + 0.083Q^{2/5}$.

The calculated entrainment rates and the experimentally determined entrainment rates are plotted in Fig. 12(a) versus Q_D^*. For comparison, the curve fits of eqns (13) and (14), and the near-field model[23] with offset, eqn (16), are plotted in Fig. 12(b). McCaffrey[5] matches the data best, coming to within $\pm 10\%$ of the data on average. However, the model does not account for the variable surrounding density, ρ_∞, which occurs in the compartment and will not be looked at further. When the variable ρ_∞ is accounted for, Baum and McCaffrey[6] match the data best coming to within -20% of the data on average. The model of Baum and McCaffrey is based on velocity and temperature measurements made in the flame and the plume above the flame for a $0.30 \, m$ square porous surface burner with heat release rates of $14 \, W$–$58 \, kW$.[38]

The lack of agreement with the models of Heskestad,[8] ρ_∞ not variable, Delichatsios[7] and Cetegen et al.[4] may be due to the differences in predicted and experimental flame heights. The larger experimental entrainment rates, compared to the models, are consistent with the lower experimental flame heights, see the Appendix. An important difference between the model of Baum and McCaffrey and the models of Heskestad, Delichatsios and Cetegen et al. is that Baum and McCaffrey do not have the burner size, D, appear explicitly in their model.

To investigate why the model of Baum and McCaffrey[6] better matches the data developed here, the flame structure measured was compared to the flame structure as represented by the model. The relevant parts of the model are:

$$m = \pi\rho_\infty U^* \sqrt{gD^*}D^{*2}R^{*2}I_{0.866} \tag{21}$$

$$z_e^* = Z_e/D$$

$$D^* = [Q/(\rho_\infty c_p T_\infty \sqrt{g})]^{2/5} = (Q/1110)^{2/5} \tag{22}$$

$$U^* = Az_e^{*p}, \qquad \theta^* = Bz_e^{*2p-1} \tag{23}$$

where, in the flame region $(0 < z^* < 1.32)$, $p = 1/2$, $A = 2.18$, and

(a)
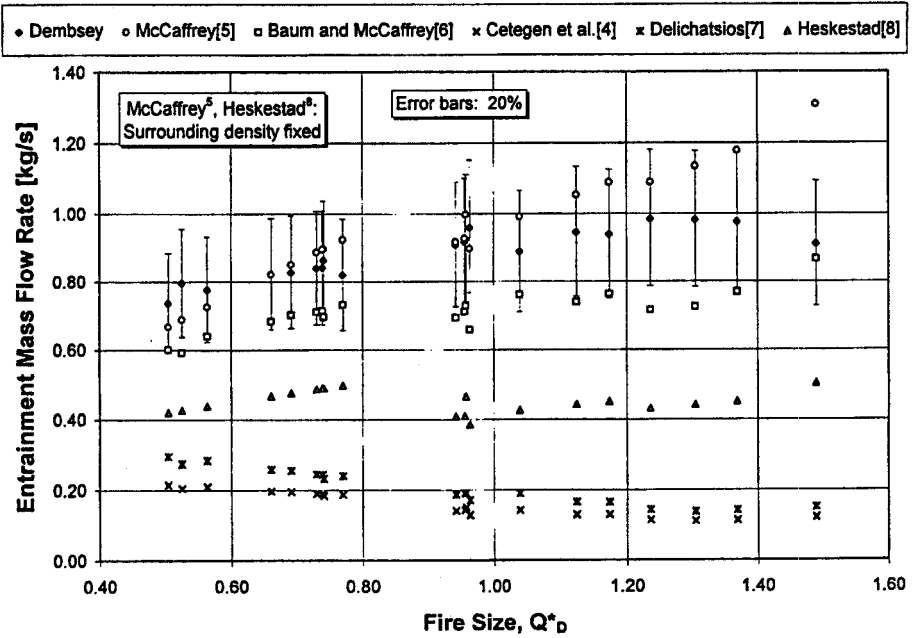
(b)
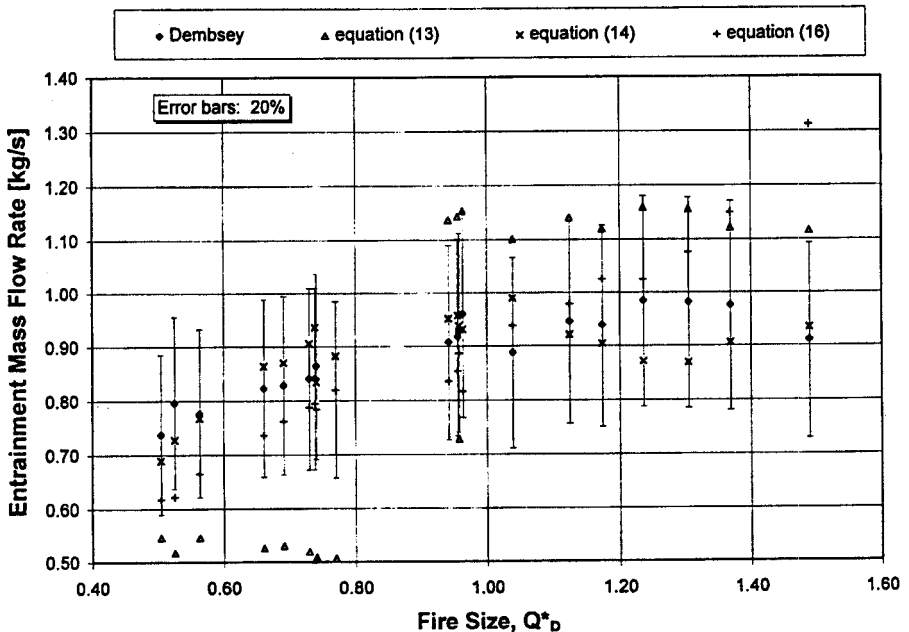
Fig. 12. (a) Experimental entrainment rate data and model[4–8] entrainment rates versus normalized fire size. The discrepancies with the models of Heskestad[8], Delichatsios[7] and Cetegen *et al.*[4] may be due to the differences in predicted and experimental flame heights; (b) experimental entrainment rate data and far-field modification curve fits, eqns (13) and (14), and near-field model[23] with offset, eqn (16), vs normalized fire size.

$B = 2.91$; in the intermittent region ($1.32 < z^* < 3.30$), $p = 0$, $A = 2.45$, and $B = 3.81$; and in the plume region ($3.30 < z^*$), $p = -1/3$, $A = 3.64$ and $B = 8.41$.

$$R^* = R/D^* = \sqrt{\frac{1-\eta}{\pi U^*(1 - I_{0.8666})}} \tag{24a}$$

for $z_e^* \geq 1.32$, and

$$R^* = R_{fl}^* = R_{fl}/D^* = \frac{\sqrt{1-\eta}}{3.65} \tag{24b}$$

for $0.66 < z_e^* < 1.32$.

$$I_{0.866} = 0.00059\theta^{*4} - 0.0508\theta^{*3} + 0.181\theta^{*2} - 0.406\theta^* + 1.00 \tag{25}$$

for $0.00 \leq \theta^* \leq 3.00$.

Baum and McCaffrey[6] do not have a burner size, D, in their model, but they do have a characteristic size of the fire, D^*, which is based on the heat release rate of the fire. Figure 13 shows the ratio $D/D^* = Q_D^{*-2/5}$ and the entrainment rates plotted versus Q_D^*. The ratio varies from 1.2 to 0.8 as Q_D^* increases. The decrease in the ratio does not seem to affect the results of the model. This is reasonable because the ratio
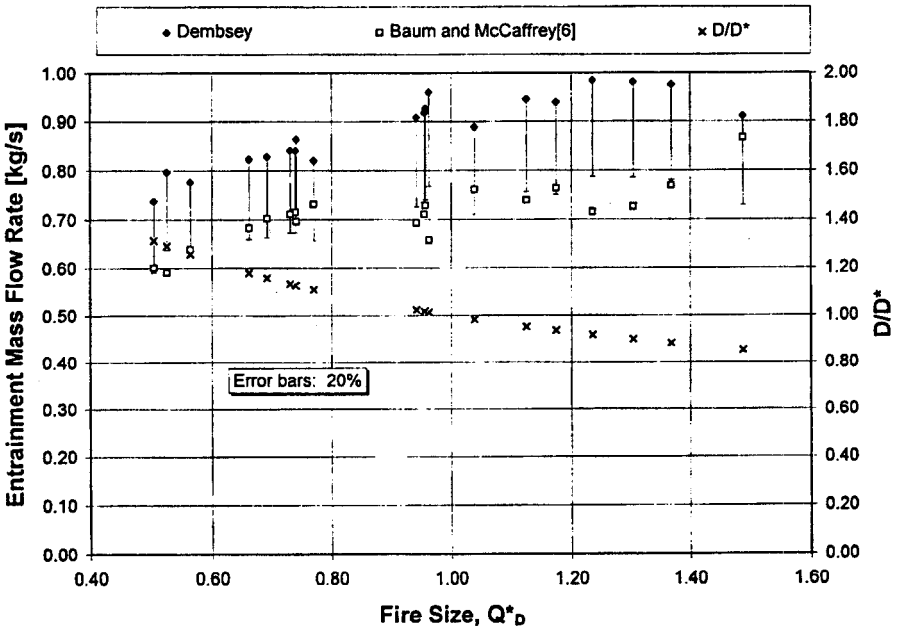
Fig. 13. Experimental and model[6] entrainment rates, and normalized burner size vs normalized fire size.

values are of order one. The ratio $D/D^* = Q_D^{*-2/5}$ of order one suggests a buoyancy driven fire which is appropriate for their model.

The normalized entrainment height, z_e^*, of each experiment is shown in Table 3. The lower limit of applicability of the model as given by Baum and McCaffrey[6] is $z_e^* = 0.66$ and that as given by McCaffrey[5] is $z_e^* = 0.38$. Once $Q_{O2} > 600 \, \text{kW}$, the lower limit of Baum and McCaffrey is surpassed. For all the experiments, the lower limit of McCaffrey is not exceeded. The results of the model do not appear to be affected by the low z_e^* values. As with the other models,[4,7,8] the flame height of Baum and McCaffrey is higher than the mean flame height as measured here, see the Appendix.

The half-widths of the flames measured at the interface, $0.5 w_{fl}$, for each experiment, normalized on the plume radius of the model, R, at the interface are shown in Table 3. The ratio increases slightly with increasing Q_{O2} and has an average value of approximately 0.8. The value of the ratio does not appear to affect the results of the model. The half-width of the flame measured is for the luminous portion only and how this relates to R is unknown. The fact that the ratio is not much greater than and/or less than 1 indicates that the model plume radius may reasonably represent the actual plume radius.

From the flame structure analysis of the model of Baum and McCaffrey,[6] it is not entirely clear why the model gives reasonable results for the entrainment data developed here. It appears that the model has approximately the correct characteristic sizes and radii of the fires. The low z_e^* values of the experiments are not a problem, however the mean flame height of the model is higher than measured.

5 CONCLUSION

Near-field entrainment rates of full-scale compartment fires ranging up to flashover and beyond, with rates between 330 and 980 kW, have been determined experimentally from a limited data set of 20 experiments. Entrainment rates of between 0.74 and 0.98 kg/s have been calculated from temperature measurements which were made in the compartment and its doorway. The temperature measurements allow the various compartment flows relevant to the entrainment rate to be determined.

The entrainment rates determined here were correlated with values from the literature[4,10–16] using a far-field model with virtual origin.[3,4] The correlation led to two curve fits for the data, eqns (13) and (14), which may be used to estimate the near-field entrainment rates over a wide range of fire sizes and heat release rates. In addition, a preliminary

offset, eqn (16), for the near-field model of Thomas[23] was quantified based on these data and those of Zukoski.[3] Existing comprehensive entrainment models[3-8] were compared to these data. It was found that the models of McCaffrey,[5] and Baum and McCaffrey[6] give the best agreement with the measured entrainment rates. The disagreement with other models[4,7,8] may be due to the differences in predicted and experimental flame heights. The model of McCaffrey[5] does not account for the changing surrounding density that exists in the compartment, so its close match to the data may be considered fortuitous. From a practical viewpoint, the close match of McCaffrey's model is important because it is the model that is used in CFAST.[1,2] This indicates that CFAST has an entrainment model that can reasonably represent full-scale compartment fires in the near field. The data set developed here, though small, suggests that to develop a comprehensive entrainment model for full-scale compartment fires, more near-field experimental data are needed over a wide range of burner and fire shapes, sizes and locations.

ACKNOWLEDGEMENT

REFERENCES

1. Portier, R. W., Reneke, P. A., Jones, W. W. & Peacock, R. D., A user's guide for CFAST version 1·6, NISTIR 4985. Building and Fire Research Laboratory, National Institute of Standards and Technology, Gaithersburg, MD, USA, 1992.
2. Peacock, R. D., Forney, G. P., Reneke, P. A., Portier, R. W. & Jones, W. W., CFAST, the consolidated model of fire growth and smoke transport, NIST Technical Note 1299. Building and Fire Research Laboratory, National Institute of Standards and Technology, Gaithersburg, MD, USA, 1993.
3. Zukoski, E. E., Mass flux in fire plumes. In *Fire Safety Science— Proceedings of the Fourth Int. Symp.* International Association for Fire Safety Science, 1994, pp. 137–47.
4. Cetegen, B. M., Zukoski, E. E. & Kubota, T., Entrainment in the near and far field of plumes. *Combust. Sci. Technol.* **39** (1984) 305–31.
5. McCaffrey, B. J., Momentum implications for buoyant diffusion flames. *Combustion and Flame*, **52** (1983) 149–67.
6. Baum, H. R. & McCaffrey, B. J., Fire induced flow field—theory and experiment. In *Fire Safety Science—Proceedings of the Second Interna-*

tional Symp. Hemisphere, New York, 1989, pp. 129–48.
7. Delichatsios, M. A., Procedure for calculating the air entrainment into turbulent pool and jet fires. *J. Fire Protection Engng*, 2 (1990) 93–8.
8. Heskestad, G., Fire plume air entrainment according to two competing assumptions. In 21*st Symp. (Int.) on Combustion*, The Combustion Institute, Pittsburgh, PA, USA, 1986, pp. 111–20.
9. Beyler, C. L., Fire plumes and ceiling jets. *Fire Safety J.*, 11 (1986) 53–75.
10. Lim, C. S., I. Mixing in doorway flows; II. Entrainment in fire plumes. Engineer's Degree Thesis, California Institute of Technology, Pasadena, CA, USA, 1984.
11. Toner, S. J., Zukoski, E. E. & Kubota, T., Entrainment, chemistry and structure of fire plumes. California Institute of Technology, Pasadena, CA, Grant Number 6ONANB6DO638, US Department· of Commerce, National Bureau of Standards, Center for Fire Research, 1986.
12. Morehart, J. H., Zukoski, E. E. & Kubota, T., Species produced in fires burning in two-layered and homogeneous vitiated environments. California Institute of Technology, Pasadena, CA, Grant Number 6ONANI3D90958, US Department of Commerce, National Institute of Standards and Technology, Center for Fire Research, 1990.
13. Tokunaga, T., Sakai, T., Kawagoe, K, Tanaka, T. & Hasemi, Y., Mass flow rate formula for the upward current above diffusion flames.· *Fire Sci. Technol.* 2 (1982) 117–25.
14. Yumoto, T. & Koseki, H., Gross structure of heptane pool fire: some experimental results. *Fire Sci. Technol.* 2 (1982) 91–7.
15. Steckler, K. D., Quintiere, J. G. & Rinkinen, W. J., Flow induced by fire in a compartment. In 19*th Symp. (Int.) on Combustion*, The Combustion Institute, Pittsburgh, PA, USA, 1982, pp. 913–20.
16. Thomas, P. H., Baldwin, R. & Heselden, A. J. M., Buoyant diffusion flames: some measurements of air entrainment, heat transfer and flame merging. In 10*th Symp. (Int.) on Combustion*, The Combustion Institute, Pittsburgh, PA, USA, 1965, pp. 983–96.
17. International Conference of Building Officials, Standard test method for evaluating room fire growth contribution of textile wall covering. In *Uniform Building Code*, Vol. 3, Int. Conf. of Building Officials, Whittier, CA, USA, Standard 8-2, 1994.
18. Thomas, P. H., Testing products and materials for their contribution to flashover in rooms. *Fire and Materials*, 5 (1981) 103–11.
19. Babrauskas, V., Upholstered furniture room fires—measurements, comparison with furniture calorimeter data, and flashover predictions. *J. Fire Sciences*, 2 (1984) 5–19.
20. Rockett, J. A., Fire induced gas flow in an enclosure. *Combust. Sci. Technol.* 12 (1976) 165–75.
21. Quintiere, J., Growth of fire in building compartments. In *Fire Standards and Safety*, ASTM STP 614, American Society for Testing and Materials, Philadelphia, PA, USA, 1977, 131–67.
22. Quintiere, J. G., Steckler, K. D. & Corley, D., An assessment of fire induced flows in compartments. *Fire Sci. Technol.* 4 (1984) 1–14.
23. Hinkley, P. L., Rates of 'production' of hot gases in roof venting experiments. *Fire Safety J.* 10 (1986) 57–65.

24. Parker, W. J., Calculations of the heat release rate by oxygen consumption for various applications, NBSIR 81-2427. Center for Fire Research, National Bureau of Standards, Washington, DC, USA, 1982.

25. Newman, J. S. & Croce, P. A., A simple aspirated thermocouple for use in fires. *J. Fire Flammability*, **10** (1979) 326–36.

26. White, F. M., *Fluid Mechanics*, 2nd ed. McGraw-Hill, New York, NY, USA, 1986, pp. 360–4.

27. ASME Research Committee on Fluid Meters, *Fluid Meters Their Theory And Application*, 5th ed. American Society of Mechanical Engineers, New York, NY, USA (1959).

28. Preston, T. S. (Ed.), *Shell Flow Meter Engineering Handbook*. Waltman, Delft, The Netherlands, 1968.

29. Spink, L. K, *Principles and Practice of Flow Meter Engineering*, 9th ed. The Foxboro Company, Foxboro, MA, USA, 1967.

30. Tewarson, A., Generation of heat and chemical compounds in fires. In *The SFPE Handbook of Fire Protection Engineering*, 1st ed., Ch. 1–13. National Fire Protection Association, Quincy, MA, USA, 1988.

31. Drysdale, D., *An Introduction to Fire Dynamics*. John Wiley, Chichester, UK, 1985, pp. 304–10.

32. Janssens, M. & Tran, H. C., Data reduction of room fire tests for zone model validation. *J. Fire Sciences*, **10** (1992) 528–55.

33. Steckler, K. D., Baum, H. R. & Quintiere, J. G., Fire induced flows through room openings—flow coefficients. In *20th Symp. (Int.) on Combustion*, The Combustion Institute, Pittsburgh, PA, USA, 1984, pp. 1591–1600.

34. Nakaya, I., Tanaka, T., Yoshida, M. & Steckler, K. D., Doorway flow induced by a propane fire. *Fire Safety J.* **10** (1986) 185–95.

35. Emmons, H. W., Vent flows. In *The SFPE Handbook of Fire Protection Engineering*, 1st ed., Ch. 1–8. Society of Fire Protection Engineers, Boston, MA, USA, 1988.

36. Jaluria, Y., Natural convection wall flows. In *The SFPE Handbook of Fire Protection Engineering*, 1st ed., Ch. 1–7, Society of Fire Protection Engineers, Boston, MA, USA, 1988.

37. Carslaw, H. S. & Jaeger, J. C., *Conduction of Heat in Solids*, 2nd ed. Oxford University Press, Oxford, UK, 1959, pp. 75–7.

38. McCaffrey, B. J., Purely buoyant diffusion flames: some experimental results, NBSIR 79-1910. Center for Fire Research, National Bureau of Standards, Washington, DC, USA (1979).

39. Cox, G. & Chitty, R., Some source-dependent effects of unbounded fires. *Combustion and Flame*, **60** (1985) 219–32.

40. Hasemi, Y. & Nishihata, M., Fuel shape effect on the deterministic properties of turbulent diffusion flames. in *Fire Safety Science—Proc. of the Second Int. Symp*, Hemisphere, New York, USA, 1989, pp. 275–84.

41. McCaffrey, B. J., Flame height. In *The SFPE Handbook of Fire Protection Engineering*, 1st ed., Ch. 1–18. Society of Fire Protection Engineers, Boston, MA, USA, 1988.

42. Hasemi, Y. & Tokunaga, T., Flame geometry effects on the buoyant plumes from turbulent diffusion flames. *Fire Sci. and Technol.*, **4** (1984) 15–26.
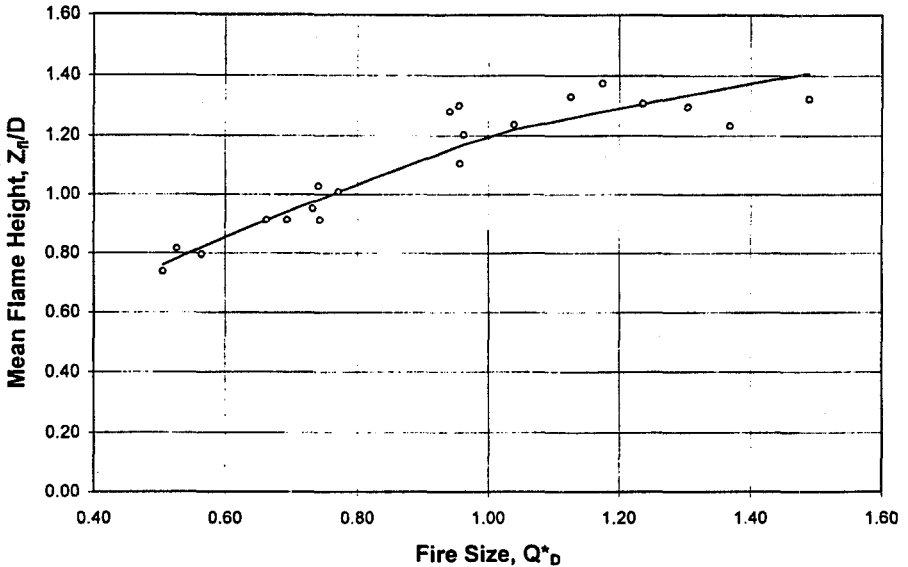
Fig. A1. Experimental normalized mean flame height vs normalized fire size. Data points and curve fit shown.

APPENDIX

A.1 Flame height: comparison to the literature

The mean flame height values of Table 2 were curve fitted using eqn (A1)[4], see Fig. A1.

$$Z_{fl}/D = \gamma Q_D^{*n} \qquad (A1)$$

$$Q_D^* = Q/(\rho_\infty c_p T_\infty \sqrt{g} D^{5/2}) Q/(1110 D^{5/2}) \qquad (A2)$$

The hydraulic diameter $D = 4A_b/P = 0.81$ m was used because of the burner configuration's rectangular shape. Use of an area equivalent diameter[8] resulted in larger scatter of the data. The best fit values of the power n were found to be $n = 2/3$ for $Q_D^* < 1$ and $n = 2/5$ for $Q_D^* > 1$. The best fit value of the constant γ was found to be 1.2.

How the curve fitted to the flame heights measured here compares with other correlations from the literature[4,6,7,39–41] is shown in Fig. A2 and in Table A1. All the correlations have been converted to a mean flame height and hydraulic diameter basis, and expressed as in eqn (A1).

Review of Fig. A2 and Table A1 shows that the square data of Hasemi and Nishihata[40] are very similar to the circular data of Cetegen
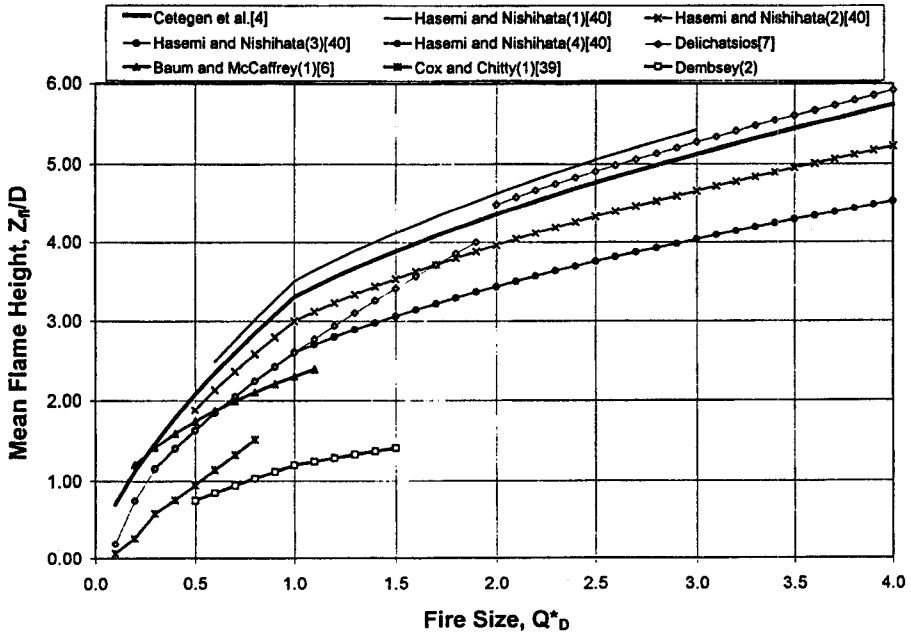
Fig. A2. Literature mean flame height correlations plotted as normalized flame height vs normalized fire size. Burner shapes (aspect ratios) are: for Cetegen *et al.*[4], circular; for Dembsey, rectangular (2); for Baum and McCaffrey,[6] square (1); for Delichatsios,[7] circular, for Cox and Chitty, square (1); and for Hasemi and Nishihata.[40], square (1) and rectangular (2, 3, 4).

et al.[4] The similarity of flame heights for square and circular burners has also been noted previously.[42] The rectangular data of Hasemi and Nishihata shows that as the aspect ratio of the burner increases, the value of γ decreases. The correlation of Delichatsios,[7] for circular burners, is similar to that of Cetegen *et al.* for $Q_D^* > 1.9$ but below 1.9, the correlation drops below that of Cetegen *et al.* and converges to the aspect ratio 3 and 4 data of Haserni and Nishihata. The correlation of Baum and McCaffrey,[6] for square burners, generally falls below that of Cetegen *et al.*, and Hasemi and Nishihata (square). The power $n = 2/5$ used by Baum and McCaffrey for $Q_D^* < 1$ is not consistent with the correlations of Hasemi and Nishihata, Cetegen *et al.*, and Delichatsios. The correlation of Cox and Chitty,[39] for square burners, falls even further below those of Cetegen *et al.* and Hasemi and Nishihata, (square).

From Fig. A2 and Table A1, the correlation determined here is lower than all the other correlations, though the power n values are consistent with Cetegen *et al.*[4] and Hasemi and Nishihata.[40] The γ value obtained here is only 40% of Hasemi and Nishihata's aspect 2 rectangular data.

TABLE A1

Literature Burner Shape, Fire Size and Mean Flame Height Correlations Based on eqn (A1)

Literature source	Burner shape (aspect ratio)	D (m)	Q (kW)	Q_D^*	n	γ
Cetegen et al.[4]	Circular	0·10, 0·19, 0·30, 0·50	3–158	0·1–1·0	2/3	3·3
Cetegen et al.[4]	Circular	0·10, 0·19, 0·30, 0·50	3–158	1·0–45	2/5	3·3
Hasemi and Nishihata[40]	Square (1)	0·20	13–60	0·6–1·0	2/3	3·5
Hasemi and Nishihata[40]	Square (1)	0·20	13–60	1·0–3·0	2/5	3·5
Hasemi and Nishihata[40]	Rectangular (2)	0·27	20–200	0·5–1·0	2/3	3·0
Hasemi and Nishihata[40]	Rectangular (2)	0·27	20–200	1·0–4·8	2/5	3·0
Hasemi and Nishihata[40]	Rectangular (3)	0·30	20–300	0·4–1·0	2/3	2·6
Hasemi and Nishihata[40]	Rectangular (3)	0·30	20–300	1·0–5·5	2/5	2·6
Hasemi and Nishihata[40]	Rectangular (4)	0·32	20–400	0·3–1·0	2/3	2·6
Hasemi and Nishihata[40]	Rectangular (4)	0·32	20–400	1·0–6·2	2/5	2·6
Delichatsios[7]	Circular	0·10, 0·19, 0·30, 0·50	3–158	<0·2	2	18·8
Delichatsios[7]	Circular	0·10, 0·19, 0·30, 0·50	3–158	0·2–1·9	2/3	2·6
Delichatsios[7]	Circular	0·10, 0·19, 0·30, 0·50	3–158	>1·9	2/5	3·4
Baum and McCaffrey[6]	Square (1)	0·30	14–58	0·2–1·1	2/5	2·3
Cox and Chitty[39]	Square (1)	0·60	46–118	0·1–0·4	2	6·5
Cox and Chitty[39]	Square (1)	0·45	57–118	0·4–0·8	1	1·9
Dembsey	Rectangular (2)	0·81	330–980	0·5–1·0	2/3	1·2
Dembsey	Rectangular (2)	0·81	330–980	1·0–1·5	2/5	1·2

Comparison to the literature does not give a clear explanation as to why the flame heights measured here are so low. The literature itself is not consistent. The data of Baum and McCaffrey,[6] and Cox and Chitty[19] as compared to Cetegen *et al.*, indicate that there is a significant effect when the shape of the burner is changed from circular to square. However, the data of Hasemi and Nishihata (square) indicates that there is no effect when the shape is changed. Additionally, the data of Baum and McCaffrey, and Cox and Chitty indicate that there is a size effect on the flame height. However, the data of Cetegen *et al.* indicate that there is no size effect.

All the literature correlations are for flames in the open, outside a compartment, and as such, any effect of the compartment on the mean flame heights measured here can not be accounted for by comparison to the literature. However, the two-layered environment and the doorway inflow of the compartment do not appear to affect the flame heights. Cetegen et al.[4] found that flame heights are not greatly different when they extend into the upper layer. The flame heights measured here appear consistent with that observation. The consistency is most clearly seen by looking at the lowest flame height, Fig. A1 and Table 2, where the flames from the 330 kW fire extend into the upper layer at $0.85Z_{fl}$. The low flame heights measured here may be a result of the size and shape of the burner used, but further exploration is needed.

A.2 Entrainment up to the flame tip

The amount of air used to burn all the fuel can be estimated by using eqn (13) to calculate the entrainment up to the flame tip. The entrainment up to the flame tip, m_{ft}, is shown in eqn (A3) and the equivalence ratio at the flame tip, ϕ_{ft}, in eqn (A4). The entrainment height at the flame tip is $Z_e = Z_{0.0} = Z_{fl}(1 + 0.5\chi)$. The mean flame height, Z_{fl}, is expressed in the general form of eqn (A1).

$$m_{ft} = \beta_{ft}(0.21\rho_\infty g^{1/2})D^{5/2}Q_D^{*1/3}(a + \gamma(1 + 0.5\chi - 0.33)Q_D^{*n})^{5/3} \quad (A3)$$

where $\beta_{ft} = \exp(0.52 - 0.26(1 + 0.5\chi))$; $\rho_\infty = 1.2 \text{ kg/m}^3$ and with floor, $a = 0.50$, without floor, $a = 0.80$.

$$\phi_{ft} = s^{-1}[m_{ft}\Delta H_c/(\rho_\infty c_p T_\infty g^{1/2}D^{5/2}Q_D^*)] = s^{-1}[m_{fl}\Delta H_c/(1110D^{5/2}Q_D^*)] \quad (A4)$$

Three cases are considered: (1) Cetegen et al. burner fires for $D = 0.50$ m; (2) the burner fires conducted here; and (3) the pool fire of Thomas et al.[16] The various input parameters are shown in Table A2. The flame structure values, γ, χ and n, for Thomas et al. are estimated based on a single mean flame height value. For each case $n = 2/3$ for $Q_D^* < 1$ and $n = 2/5$ for $Q_D^* > 1$.

For fire sizes $0.5 < Q_D^* < 1.5$, the average values of ϕ_{ft} were: for Cetegen et al.[4], $\phi_{ft} = 22$; for Dembsey, $\phi_{ft} = 7.9$; and for Thomas et al.,[16] $\phi_{ft} = 14$, see Table A2. Cetegen et al. measured an average value of $\phi_{ft} = 18$ with a variation of ±30%. From the measurements of Thomas et al., an estimate of $\phi_{ft} = 12$ was made. The estimates from eqn (A4) compare favorably with these values.

The ϕ_{ft} values for the three cases indicate that as the size of the burner or pool is increased above $D = 0.50$ m, better mixing of the fuel

TABLE A2

Input parameters For Flame Tip Entrainment Calculation, eqns (A3) and (A4), and Calculated Flame Tip Equivalence Ratios for Three Cases: Cetegen *et al.*,[4] Dembsey, and Thomas *et al.*[16]

	Cetegen et al.[4]	*Dembsey*	*Thomas* et al.[16]
Inputs			
Fuel	City gas	Propane	Alcohol
D (m)	0·50	0·81	0·91
γ	3·3	1·2	2·4
χ	0·75	0·67	0·70
a	0·50	0·80	0·50
ΔH_c (MJ/kg)	48	46·4	27
s	17	15·6	9·1
Output			
Average ϕ_{ft}^*	22	7·9	14

* Fire sizes $0·5 < Q_D^* < 1·5$.

and air occurs in the flames. The difference in ϕ_{ft} values between Thomas *et al.* [16] and the experiments conducted here indicate that there may be a shape effect as well. This is consistent with the data of Hasemi and Nishihata,[40] Table A1 and Fig. A2. Hasemi and Nishihata measured a 14% drop in flame height when the burner shape was changed from square to an aspect ratio 2 rectangle. The difference between Thomas *et al.* and the experiments here suggest that for $D > 0·50$ m burners, the drop may be 50% in flame height and 44% in ϕ_{ft}, indicating that the shape effect may be more significant for larger burners. As was discussed with respect to flame heights, the compartment does not appear to affect the flame tip entrainment measured here because the doorway does not limit the inflow of air, no bent-over plumes were observed and the lower-layer temperature was accounted for in eqn (13).